

Constraints on the velocity profiles of galaxies from strong lensing statistics and semi-analytical modelling of galaxy formation

Kyu-Hyun Chae,^{1*} Shude Mao² and Xi Kang³

¹*Sejong University, Department of Astronomy and Space Sciences, 98 Gunja-dong, Gwangjin-Gu, Seoul 143-747, Republic of Korea*

²*University of Manchester, Jodrell Bank Observatory, Macclesfield, Cheshire SK11 9DL, UK*

³*Astrophysics Department, University of Oxford, Keble Road, Oxford OX1 3RH, UK*

Accepted Received; in original form

ABSTRACT

Semi-analytical models of galaxy formation can be used to predict the evolution of the number density of early-type galaxies as a function of the circular velocity at the virial radius, $v_{c,\text{vir}}$. Gravitational lensing probability and separation distribution on the other hand are sensitive to the velocity dispersion (or circular velocity) at about the effective radius. We adopt the singular isothermal ellipsoid (SIE) lens model to estimate the velocity dispersion at the effective radius. The velocity dispersion from strong lensing based on the SIE, σ_{SIE} is then closely related to the observational central stellar velocity dispersion, σ_{cent} ; we have empirically $\sigma_{\text{SIE}} \approx \sigma_{\text{cent}}$. We use radio lenses from the Cosmic Lens All-Sky Survey and the PMN-NVSS Extragalactic Lens Survey to study how the velocity dispersions, σ_{SIE} , are related to $v_{c,\text{vir}}$; if the galaxy were a singular isothermal sphere up to the virial radius, $v_{c,\text{vir}} = \sqrt{2}\sigma_{\text{SIE}}$. When we include both the lensing probability and separation distribution as our lensing constraints, we find $\sigma_{\text{SIE}}/(200 \text{ km s}^{-1}) = [(1.17_{-0.26}^{+0.40})v_{c,\text{vir}}/(200 \text{ km s}^{-1})]^{0.22^{+0.05}_{-0.04}}$ for $200 \text{ km s}^{-1} \lesssim \sigma_{\text{SIE}} \lesssim 260 \text{ km s}^{-1}$; at $\sigma_{\text{SIE}} = 200 \text{ km s}^{-1}$, the ratio $\sqrt{2}\sigma_{\text{SIE}}/v_{c,\text{vir}}$ is about $1.65_{-0.37}^{+0.57}$ (68% CL) but decreases to $0.65_{-0.12}^{+0.15}$ (68% CL) for $\sigma_{\text{SIE}} = 260 \text{ km s}^{-1}$. These results are consistent with those of Seljak (2002) obtained from galaxy-galaxy weak lensing for galaxies of around L_* . However, our results clearly suggest that the ratio must vary significantly as σ_{SIE} is varied and are marginally discrepant with the Seljak results at $\sigma_{\text{SIE}} = 260 \text{ km s}^{-1}$. The scaling $\sigma_{\text{SIE}} \propto v_{c,\text{vir}}^{0.22 \pm 0.05}$ is broadly consistent with those from galaxy occupation statistics studies and the most recent galaxy-galaxy weak lensing study. We discuss briefly the implications of our results for galaxy formations and structures. These constraints can be significantly strengthened when larger lens samples become available and the accuracy of semi-analytical model predictions improves.

Key words: gravitational lensing – galaxies: formation – galaxies: haloes – galaxies: kinematics and dynamics – galaxies: structure

1 INTRODUCTION

The Λ CDM structure formation model has been very successful in explaining many observations, for example the cosmic microwave background radiation (Spergel et al. 2003, 2006), and the large-scale structures (Peacock et al. 2001; Tegmark et al. 2004). In this model, the tiny quantum fluctuations in the early universe are amplified due to gravitational instabilities, and eventually evolve into

highly nonlinear structures. The dissipationless cold dark matter dominates the gravity, and determines the basic abundance, the internal structure and formation history of the nonlinear dark matter haloes. Such information can be reliably obtained using N -body simulations and/or analytical models such as the Press-Schechter formalism (e.g., Press & Schechter 1974; Sheth & Tormen 2002). For example, the dark matter haloes follow approximately the Navarro, Frenk and White (NFW) profile (Navarro et al. 1997, 2004), and their shapes can be approximated by tri-axial ellipsoidal models (Jing & Suto

* chae@sejong.ac.kr

2002). Their time evolution can be studied numerically, which is also matched well by the analytical extended Press-Schechter formalism (e.g., Bond et al. 1991; Lacey & Cole 1994; Sheth & Tormen 2002),

On the other hand, the visible galaxies we see today are formed by the condensation of baryons within dark matter haloes due to radiative processes. When the baryons sink toward the centre of dark haloes and become self-gravitating, star formation, active galactic nuclei and feedback processes will occur. Unfortunately, these phenomena are not well-understood. For clusters of galaxies, baryonic cooling is not very important, so their mass profiles still approximately follow the predictions from N -body simulations, as seen from kinematic (e.g., van der Marel et al. 2000), lensing (e.g., Comerford et al. 2006) and X-ray (Voigt & Fabian 2006) studies of clusters of galaxies. On the scale of galaxies, cooling is important, and the central profiles of galaxies are likely to be significantly affected by baryonic processes. Hydrodynamical high-resolution simulations can now simulate regions of the universe or individual galaxies (e.g., Meza et al. 2003), but they cannot yet resolve the internal structure of galaxies and at the same time simulate large enough volume to be statistically representative (and realistic). Nevertheless, rapid progress has been made, including more realistic modelling of the multi-phase interstellar medium (Springel & Hernquist 2003). An alternative approach is to use semi-analytical studies which can incorporate many physical processes in an intuitive way (Kauffmann et al. 1999; Somerville & Primack 1999; Cole et al. 2000; Kang et al. 2005; Croton et al. 2006). These models can reproduce the luminosity function and correlation function of galaxies reasonably well. However, although these models can provide the number of galaxies as a function of circular velocity at the virial radius, they cannot yet reliably predict the central dynamical properties of galaxies, such as the central velocity dispersions.

The central velocity dispersions (or the velocity dispersions in the optical regions) of galaxies are precisely the information needed for the studies of gravitational lensing, as the lensing probability is proportional to σ^4 while the image separation is proportional to σ^2 . Earlier studies (e.g., Narayan & White 1988; Kochanek 1995) used singular isothermal spheres to constrain variants of CDM models. In this scenario, the velocity dispersion is simply related to the circular velocity at the virial radius by $v_c = \sqrt{2}\sigma$. However, this assumption is likely to be invalid for two reasons. The NFW profile for haloes does not give rise to a flat rotation curve. In fact, the value of its peak is about 20 per cent higher than that at the virial radius for a concentration parameter (≈ 10) appropriate for Milky-Way sized haloes. Second, the baryons settled at the centre may further increase the central rotations and velocity dispersions. As the assembly of galaxies is not yet well understood, how the velocity dispersion in the optical region relates to the virial circular velocity is therefore a parameter we want to extract from observations. In this paper, we propose to use strong gravitational lensing to constrain this key parameter.

At the time of this writing no study has made use of the predictions of semi-analytical studies of galaxy abundances of different types. Several studies have used gravitational lensing to constrain the evolution of galaxies (Mao 1991; Mao & Kochanek 1994; Ofek et al. 2003; Chae & Mao

2003). In this paper, we will use the predicted abundance of ellipticals from semi-analytical models as a function of virial circular velocity. We then adopt a simple form to parameterise the relation between the velocity dispersion at the optical radius and the circular velocity at the virial radius. We use radio lenses from the Cosmic Lens All-Sky Survey (CLASS; Myers et al. 2003; Browne et al. 2003) and the PMN-NVSS Extragalactic Lens Survey (PANELS; Winn et al. 2001b) to constrain this factor empirically. This in turn will provide an important way of understanding the baryonic effects on the central properties of galaxies. Our approach is independent of the galaxy-galaxy weak lensing studies of the same factor (Seljak 2002), who found that for both early-type and late-type galaxies around L_* , their peak velocities are about a factor from 1.7 to 1.8 (with an uncertainty of about 20%) of the circular velocity at the virial radius. The structure of this paper is as follows. In §2, we outline our method and the data to be used. In §3, we present the results of our analyses. Finally, in §4 we discuss the implications of our results for galaxy formation along with possible sources of systematic errors and give the main conclusions of our study.

2 MODEL, METHOD AND DATA

In §2.1 we introduce velocity functions of galaxies starting from the Schechter luminosity function (Schechter 1976) of galaxies. We also adopt a model for the relation between the velocity dispersion arising from strong lensing and the virial circular velocity predicted from semi-analytical modelling of galaxy formation (§2.1). In §2.2 we briefly describe our adopted semi-analytical model (SAM) of galaxy formation and present simulated data to be used in this work. We also outline our formalism of strong lensing statistics to constrain the radial velocity profile of galaxies based on the SAM circular velocity function and strong lensing data.

2.1 Velocity functions of galaxies

The number density of galaxies as a function of luminosity is described by the Schechter luminosity function (LF) ϕ_L given by

$$dn = \phi_L(L)dL = \phi_* \left(\frac{L}{L_*}\right)^{\alpha_L} \exp\left(-\frac{L}{L_*}\right) \frac{dL}{L_*}. \quad (1)$$

We assume an effective power-law relation between the luminosity (L) and the velocity dispersion (σ) for the scale under consideration of galaxies given by¹

$$\frac{L}{L_*} = \left(\frac{\sigma}{\sigma_*}\right)^{\beta_{VD}}. \quad (2)$$

Then the number density of galaxies as a function of velocity dispersion can be described by the velocity dispersion function (VDF) ϕ_{VD} given by

¹ In reality the relation between L and σ does not follow an exact power-law relation but suffers from a significant scatter. Thus, the power-law fitting function between L and σ , namely the Faber-Jackson relation (Faber & Jackson 1976), may not be the same as this effective relation (see Sheth et al. 2003).

Table 1. Summary of velocity and related parameters

parameter	meaning	relevant scale
$v_{c,\text{vir}}$	circular velocity at the virial radius	r_{vir}
$v_{c,\text{eff}}$	circular velocity at the effective radius	r_{eff}
σ_{mod}	lens model velocity dispersion	$\sim r_{\text{eff}}$
(σ_{SIE})	(SIE model velocity dispersion)	
σ_{cent}	observed central velocity dispersion	$\lesssim r_{\text{eff}}$
$\sqrt{2}\sigma_{\text{SIE}}$	SIE model circular velocity	$\sim r_{\text{eff}}$
η	$\equiv \sigma_{\text{mod}}/\sigma_{\text{cent}}$	
f	$\equiv \sigma_{\text{mod}}/v_{c,\text{vir}}$	

Notes. r_{vir} = virial radius. r_{eff} = effective radius.

$$dn = \phi_{\text{VD}}(\sigma)d\sigma = \phi_* \left(\frac{\sigma}{\sigma_*}\right)^{\alpha_{\text{VD}}-1} \exp\left[-\left(\frac{\sigma}{\sigma_*}\right)^{\beta_{\text{VD}}}\right] \beta_{\text{VD}} \frac{d\sigma}{\sigma_*}, \quad (3)$$

where $\alpha_{\text{VD}} = (\alpha_{\text{L}} + 1)\beta_{\text{VD}}$.

In this work we shall study how the velocity dispersion in the optical region and the inner halo constrained by strong lensing statistics is related to the circular velocity at the virial radius ($v_{c,\text{vir}}$) predicted by an up-to-date semi-analytical model of galaxy formation. Notice that the velocity dispersion constrained by strong lensing depends on the adopted lens model (e.g., Chae 2003). We shall denote the lens model-dependent velocity dispersion by σ_{mod} . Parameter σ_{mod} corresponds to the velocity dispersion approximately at the scale of the optical region and the inner part of the halo because the observed galactic-scale lens images are formed at around the effective radii. In particular, although a lens model may imply a mass distribution from the galactic centre to infinity, the mass distribution well outside the optical region is an extrapolation that is not sensitive to strong lensing. We expect that the velocity dispersion σ_{mod} is closely related to the central stellar velocity dispersion, σ_{cent} that is observable in the aperture-limited spectroscopic observations. In this work we shall assume a constant proportionality between the two parameters; we write

$$\sigma_{\text{mod}} = \eta\sigma_{\text{cent}} \quad (4)$$

(see §4 for a discussion on the possibilities of varying η).

Hereafter for the sake of simplicity parameters σ and v_c shall refer respectively to σ_{mod} and $v_{c,\text{vir}}$ unless specified otherwise. We parameterise the relationship between the two parameters σ and v_c by

$$\sigma = f(v_c)v_c. \quad (5)$$

This is reasonable as on the cluster scale, the baryonic effect may be small, while the baryonic condensation within galactic-sized halos may significantly boost the velocity dispersion in the optical region relative to the virial circular velocity. We adopt a model given by

$$f(v_c) = f_* \left(\frac{v_c}{v_{c*}}\right)^\mu, \quad (6)$$

where $\mu = 0$ corresponds to the case where the velocity dispersion is related to the virial circular velocity by a constant proportionality. For the above model of equation (6)

the virial circular velocity function (CVF) ϕ_{CV} takes the following form²

$$dn = \phi_{\text{CV}}(v_c)dv_c = \phi_* \left(\frac{v_c}{v_{c*}}\right)^{\alpha_{\text{CV}}-1} \exp\left[-\left(\frac{v_c}{v_{c*}}\right)^{\beta_{\text{CV}}}\right] \beta_{\text{CV}} \frac{dv_c}{v_{c*}}, \quad (7)$$

where we have the following relations:

$$\alpha_{\text{CV}} = \alpha_{\text{VD}}(\mu+1), \quad \beta_{\text{CV}} = \beta_{\text{VD}}(\mu+1), \quad \text{and} \quad \sigma_* = f_*v_{c*}. \quad (8)$$

The above CVF (equation 7) implies an effective power-law relation between the luminosity and the virial circular velocity of galaxies given by

$$\frac{L}{L_*} = \left(\frac{v_c}{v_{c*}}\right)^{\beta_{\text{CV}}}. \quad (9)$$

The velocity and related parameters introduced above are summarised in Table 1.

Finally, a galaxy of v_{c*} may not correspond to a typical L_* galaxy. Suppose an L_* galaxy has a velocity dispersion of σ_0 . Then the value of f (equation 6) for σ_0 is given by

$$f_0 = f_* \left(\frac{\sigma_0}{\sigma_*}\right)^{\mu/(\mu+1)}. \quad (10)$$

We shall use parameter f_0 rather than f_* for a chosen value of σ_0 .

2.2 Strong lensing statistics and semi-analytical model of galaxy formation

The statistical properties of strong lensing are determined by four ingredients, namely the number density of potential lenses as a function of redshift, the lens cross sections, the cosmology, and the magnification bias depending on the potential source population (see, e.g., Chae 2003). Most studies of strong lensing statistics have used the present-day galaxy population given in the form of luminosity (or velocity dispersion) function for the number density of potential lenses (see, e.g., Turner et al. 1984; Fukugita et al. 1992; Kochanek 1996; Helbig et al. 1999; Chae 2003; Mitchell et al. 2005). In this paper, however, we adopt the number density of galaxies from the recent semi-analytical model of Kang et al. (2005), which gives the number density of galaxies as a function of redshift and the circular velocity at the virial radius.

The galaxy catalogue constructed by Kang et al. (2005) used a high-resolution N-body simulation by Jing & Suto (2002). The simulation follows the evolution of 512^3 particles in a cosmological box of $100h^{-1}\text{Mpc}$ with the standard concordance cosmological model ($\Omega_{\text{m},0} = 0.3, \Omega_{\Lambda,0} = 0.7, \sigma_8 = 0.9, h = 0.7$). Kang et al. (2005) adopted reasonable treatment of physical processes in predicting galaxy population such as cooling, star formation rate and energy feedbacks from supernova, and dust extinction. The parameters in the model were normalized by the local galaxy luminosity functions. The readers are referred to that paper for more detail.

The Kang et al. (2005) SAM reproduces the luminosity function of galaxies reasonably well for the range of luminosity suitable for strong lensing studies. The semi-analytical studies provide a simple way of dividing galaxies

² This particular form is the same functional form as the VDF given by equation (3). This is the direct consequence of adopting the particular model of equation (6).

Table 2. Distribution of the number of early-type and late-type galaxies as a function of virial circular velocity predicted by the Kang et al. (2005) semi-analytical model of galaxy-formation. Each value given here is the number of early-type (late-type) galaxies in a velocity bin of width 25 km s^{-1} contained within a total comoving volume of $10 \times 10^6 h^{-3} \text{ Mpc}^3$ distributed for the redshift range of $0.3 \lesssim z \lesssim 1$.

i (bin #)	$v_{c,\text{vir}}(i)$ (km s $^{-1}$) (mean virial circular velocity)	$\Delta N^{(\text{early})}(i)$ (# of early-type galaxies)	$\Delta N^{(\text{late})}(i)$ (# of late-type galaxies)
1	112.5	30321	148585
2	137.5	12854	73322
3	162.5	5816	40381
4	187.5	2789	22903
5	212.5	1719	14661
6	237.5	1377	8802
7	262.5	1266	5899
8	287.5	830	3808
9	312.5	763	2357
10	337.5	688	1484
11	375.	532	830
12	425.	295	442
13	475.	186	260
14	525.	145	120
15	575.	108	72

Table 3. Strongly lensed systems from the CLASS (Browne et al. 2003) and the PANELS southern sky (Winn et al. 2000, 2001a,b, 2002a,b) radio surveys (taken from Chae 2005). The systems under the ‘CLASS statistical’ survey are members of the well-defined CLASS statistical sample of 8958 radio sources (Browne et al. 2003; Chae 2003).

Source	Survey	Source Redshift	Lens Redshift	Image Separation (arcsec)	Image Multiplicity	Lens Type
B0128+437	CLASS	3.124	1.145	0.54	4	unknown
J0134–0931	PANELS	2.225	0.7645	0.681	2+4	2Gs
B0218+357	CLASS statistical	0.96	0.68	0.334	2	spiral
B0414+054	CLASS	2.62	0.958	2.09	4	early-type
B0445+123	CLASS statistical	—	0.558	1.33	2	early-type
B0631+519	CLASS statistical	—	0.620	1.16	2	early-type
B0712+472	CLASS statistical	1.34	0.41	1.27	4	early-type
B0739+366	CLASS	—	—	0.54	2	unknown
B0850+054	CLASS statistical	—	0.588	0.68	2	spiral
B1030+074	CLASS	1.535	0.599	1.56	2	early-type
B1127+385	CLASS	—	—	0.70	2	spiral
B1152+199	CLASS statistical	1.019	0.439	1.56	2	unknown
B1359+154	CLASS statistical	3.235	—	1.65	6	3Gs
B1422+231	CLASS statistical	3.62	0.34	1.28	4	early-type
B1555+375	CLASS	—	—	0.42	4	unknown
B1600+434	CLASS	1.57	0.415	1.39	2	spiral
B1608+656	CLASS statistical	1.39	0.64	2.08	4	2Gs
J1632–0033	PANELS	3.42	1	1.47	2	early-type
J1838–3427	PANELS	2.78	0.36	1.0	2	early-type
B1933+503	CLASS statistical	2.62	0.755	1.17	4	early-type
B1938+666	CLASS	$\gtrsim 1.8$	0.881	0.93	ring	early-type
J2004–1349	PANELS	—	—	1.13	2	spiral
B2045+265	CLASS statistical	—	0.867	1.86	4	puzzling
B2108+213	CLASS	—	0.365	4.55	2 or 3	2Gs+cluster
B2114+022	CLASS statistical	—	0.32/0.59	2.57	2	2Gs
B2319+051	CLASS statistical	—	0.624/0.588	1.36	2	early-type

into two populations, namely the early-type (ellipticals and S0’s) population and the late-type population based on the correlation between the B-band bulge-to-disk ratio and the Hubble type of the galaxy (Simien & de Vaucouleurs 1986). We use only the early-type population for this work because the radio lens sample we shall use contains only a small num-

ber of spiral lensing galaxies. Table 2 shows the numbers of early-type and late-type galaxies in velocity bins contained in $10 \times 10^6 h^{-3} \text{ Mpc}^3$ volume distributed for the redshift range of $0.3 \lesssim z \lesssim 1$.

While the SAM data can give a virial circular velocity function, strong lensing is not sensitive to the virial circu-

lar velocity but the velocity dispersion in the optical region and the inner halo. Hence to proceed in lensing computations using the number density of early-type galaxies from the SAM we must relate the virial circular velocity to the velocity dispersion. We proceed as follows. We adopt the VDF $\phi_{\text{VD}}(\sigma)$ (equation 3) for lensing computations and the CVF $\phi_{\text{CV}}(v_c)$ (equation 7) for describing the SAM data assuming that they are related by the power-law model given by equation (6). We then fit lensing data and the SAM data simultaneously. To fit the VDF to lensing data we use a maximum likelihood method based on those recently used by Chae et al. (2002), Chae (2003) and Chae (2005). The likelihood for lensing is defined by

$$\ln \mathcal{L} = \left(\sum_{j=1}^{N_{\text{IS}}} w_j \ln \delta p_{\text{IS}}(j) \right) + \left(\sum_{k=1}^{N_{\text{U}}} \ln[1 - p(k)] + \sum_{l=1}^{N_{\text{L}}} \ln \delta p(l) \right), \quad (11)$$

where the first term is the likelihood due to the relative image separation probabilities of lensed sources as defined by Chae (2005) and the terms in the second parenthesis are the likelihood due to the CLASS statistical sample (Browne et al. 2003) as defined by Chae et al. (2002) and Chae (2003); parameters w_k are the weight factors, $\delta p_{\text{IS}}(j)$ (equation 4 of Chae 2005) are the relative image separation probabilities for lensed sources with well-defined image separations (Table 3; see also Table 1 of Chae 2005), $p(k)$ (equation 40 of Chae 2003) are the total lensing probabilities for the unlensed sources in the CLASS statistical sample (see §3.1 and §3.2 of Chae 2003), and $\delta p(l)$ (equations 29, 38, or 39 of Chae 2003) are the differential lensing probabilities for the lensed sources in the CLASS statistical sample (Table 3; see also Table 1 of Chae 2003). Notice that the above lensing probabilities are calculated assuming the singular isothermal ellipsoid (SIE) lens model whose projected surface density is given by (Chae 2003)

$$\Sigma_{\text{SIE}}(x, y) = \frac{\sigma_{\text{SIE}}^2}{2G} \frac{\sqrt{e}\lambda(e)}{\sqrt{x^2 + e^2y^2}}, \quad (12)$$

where σ_{SIE} is the model velocity dispersion, e is the axis ratio, and $\lambda(e)$ is the ‘dynamical normalisation’ factor (§ 2.1.1 of Chae 2003). We assume that galaxies are not biased toward either oblate or prolate shape and have a mean projected ellipticity of $\epsilon (\equiv 1 - e) \lesssim 0.45$ so that $\lambda(e) \approx 1$. Notice that the shape and characteristic velocity dispersion of the VDF are most directly constrained by the image separation distribution. The absolute lensing probability of the CLASS statistical sample is also sensitive to the VDF as the lensing probability is proportional to $\phi_* \sigma_*^4$. The chi-squared for lensing is then defined by

$$\chi_{\text{lens}}^2 = -2 \ln \mathcal{L}. \quad (13)$$

To fit the CVF (equation 7) to the SAM data (Table 2) we define the following chi-squared function

$$\chi_{\text{SAM}}^2 = \sum_{i=1}^{N_{\text{bin}}} \left(\frac{\phi_{\text{CV}}(v_c(i)) \Delta v_c \Delta V - \Delta N(i)}{\sqrt{\Delta N(i)}} \right)^2, \quad (14)$$

where $\Delta v_c = 25 \text{ km s}^{-1}$ and $\Delta V = 10^7 \text{ h}^{-3} \text{ Mpc}^3$. Finally, the total chi-squared function is defined to be

$$\chi_{\text{tot}}^2 = \chi_{\text{lens}}^2 + \chi_{\text{SAM}}^2. \quad (15)$$

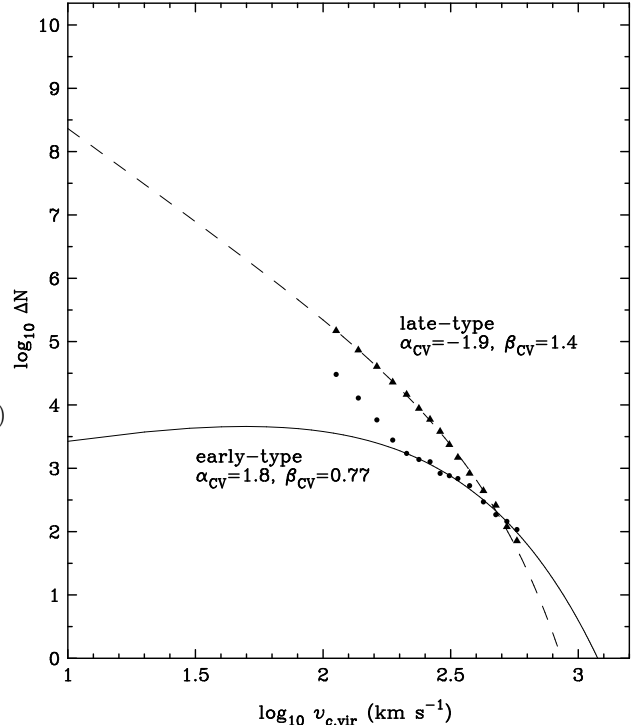


Figure 1. The numbers of early-type galaxies and late-type galaxies (Table 2) as a function of circular velocity at the virial radius predicted by the Kang et al. (2005) semi-analytical model of galaxy formation. The circular velocity functions fitted to the data using equation (7) are also shown. We have used Poisson errors for the fitting, which are however too small to display, and ignored the first four data points of the early-type population (see the texts). The results are for $10 \times 10^6 \text{ h}^{-3} \text{ Mpc}^3$ comoving volume nearly uniformly distributed over the redshift range of $0.3 \lesssim z \lesssim 1$. The velocity bin size is 25 km s^{-1} .

3 RESULTS

We first examine the simulated data from the Kang et al. (2005) SAM. Fig. 1 shows the SAM data points (Table 2) along with the fitted CVFs (equation 7) through the chi-squared function given by equation (14). Notice that the lowest 4 data points for the early-type population are not included in the fitting because they do significantly deviate from the behaviour of the rest of the data points. We shall not use these 4 data points in our study of the velocity profile of early-type galaxies (see below and §4). Fig. 2 shows the constraints on the shapes of the CVFs and compares with the shape of the VDF of the early-type population obtained by Chae (2005). Notice that the CVF shape is significantly different from the VDF shape for the early-type population. This means that the velocity dispersion cannot be related to the virial circular velocity by a constant proportionality (i.e. the case $\mu = 0$ in equation 6).

We simultaneously fit the VDF (equation 3) and the CVF (equation 7) for the early-type galaxy population assuming the relation between the two given by equations (5) and (6) to the lensing data and the SAM data by minimising the total chi-squared function χ_{tot}^2 given by equation (15). We do not use the first 4 data points ($i = 1$ to

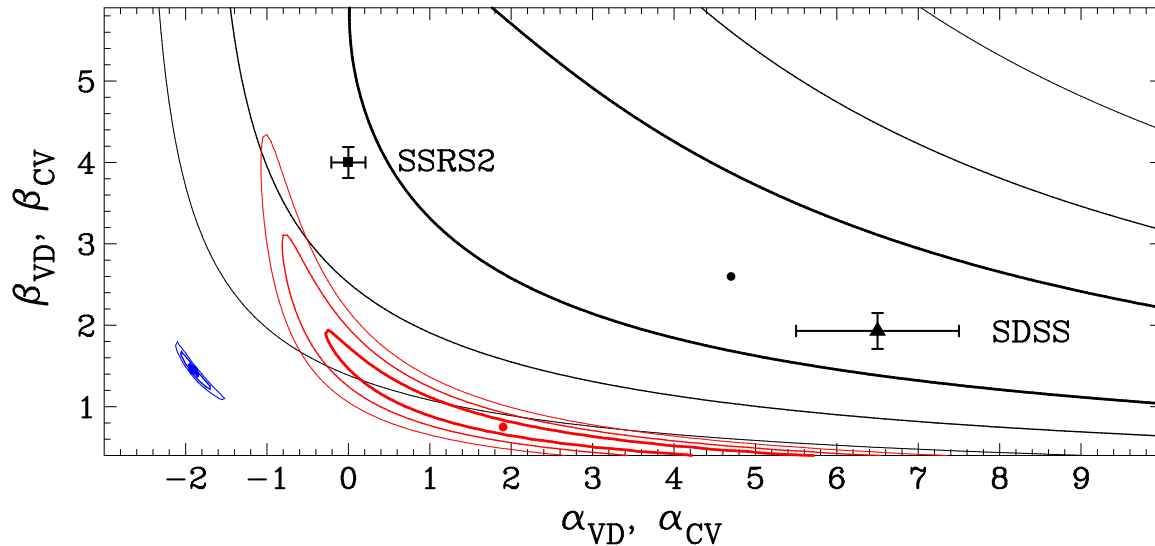


Figure 2. Constraints on the velocity functions of galaxies. The red and blue contours are respectively the confidence limits (CLs) on the CVFs (equation 7) for the early-type and the late-type populations as obtained from the Kang et al. (2005) SAM simulated data. The black contours are the CLs on the VDF (equation 3) for the early-type population as obtained by Chae (2005) from the image separation distribution of gravitational lenses. The three contours on each function correspond respectively to 1σ , 2σ , and 3σ . The filled triangle represents the SDSS VDF as obtained by Sheth et al. (2003) from the measured central velocity dispersions of early-type galaxies. The filled square represents the SSRS2 VDF as obtained by Chae (2003) from the Marzke et al. (1998) early-type LF and a measured Faber-Jackson relation.

4 in Table 2) for the early-type population from the SAM. These 4 data points do not fit into the model CVF (equation 7) while all the rest do (Fig. 1). These data points might be an artifact due to the currently imperfect SAM of Kang et al. (2005) (see §4). Perhaps, more importantly, lowest velocity galaxies may not be effective for strong lensing for the following two reasons: the lensing cross-section scales as σ_{SIE}^4 and their inner mass profiles may be too shallow (e.g., de Blok 2005, see, however, Swaters et al. 2003). So simply ignoring them would make small errors in our study. Nevertheless, we must bear in mind that any of our derived results for $v_{c,\text{vir}} \lesssim 190 \text{ km s}^{-1}$ will be an extrapolation and the strict range of validity for our analyses is $200 \text{ km s}^{-1} \lesssim v_{c,\text{vir}} \lesssim 600 \text{ km s}^{-1}$ (see Table 2).

We consider first the case where we use both of the parts in equation (11), namely both the relative image separation probabilities and the lensing properties of the CLASS statistical sample. For the CLASS statistical sample (Browne et al. 2003; Chae 2003) the number of sources that are not strongly lensed is $N_{\text{U}} = 8945$. There are 13 strongly lensed sources in the CLASS statistical sample as can be found in Table 3. However, the lenses for B0218+357 and B0850+054 are spiral galaxies and the system B2045+265 might include a spiral galaxy (or spiral galaxies) but its lensing interpretation remains puzzling (see Fassnacht et al. 1999). Excluding these three sources we take $N_{\text{L}} = 10$ for lensing solely due to the early-type galaxy population. To be included in the likelihood as relative image separation probabilities are B0414+054, B1030+074, J1632-0033, J1838-3427 and B1938+666, each of which is known to be strongly lensed by a single early-type galaxy, and B0128+437, B0739+366 and B1555+375 whose lens

types are unknown. For the last three sources we take $w_k = 0.8$ while $w_k = 1$ for the rest. Notice that the lensed sources of the CLASS statistical sample are not included in the likelihood of the relative image separation probabilities because the likelihood of the CLASS statistical sample includes the relative image separation probabilities as well as the absolute lensing probability (see, e.g., Chae 2003). Fig. 3 shows the confidence limits in the plane of μ (equation 6) and $\sqrt{2}f_0$ (equation 10). Here we have chosen $\sigma_{\text{SIE}0} = 200 \text{ km s}^{-1}$ for the fiducial velocity dispersion. Fig. 4 shows how the factor $\sqrt{2}f (= \sqrt{2}\sigma_{\text{SIE}}/v_{c,\text{vir}})$ behaves as the velocity dispersion (σ_{SIE}) is varied. Notice that $\sqrt{2}\sigma_{\text{SIE}}$ would be equal to the circular velocity in the optical region if the galaxy mass profile were isothermal up to a few effective radii. The quantity $\sqrt{2}\sigma_{\text{SIE}}$ will thus be our estimate of the circular velocity at the effective radius $v_{c,\text{eff}}$ from strong lensing based on the SIE model (equation 12). To understand better Fig. 4 it is useful to rewrite f as

$$f = f_0 \left(\frac{\sigma_{\text{SIE}}}{\sigma_{\text{SIE}0}} \right)^{\mu/(\mu+1)}, \quad (16)$$

which can be derived from equation (6) using equation (10). From equation (16) we can see that for the given uncertainties of μ and f_0 (Fig. 3) the uncertainty of f increases as σ_{SIE} decreases since μ is negative. We can equivalently say that the uncertainty of the ratio $f = \sigma_{\text{SIE}}/v_{c,\text{vir}}$ increases as σ_{SIE} (and thus $v_{c,\text{vir}}$) decreases for a given uncertainty of $v_{c,\text{vir}}$. Finally, Fig. 5 (Fig. 6) shows how $v_{c,\text{vir}}$ (σ_{SIE}) behaves as σ_{SIE} ($v_{c,\text{vir}}$) is varied.

Next we consider the case where we use only the first part in equation (11), namely the relative image separation probabilities. Notice that in this case the absolute

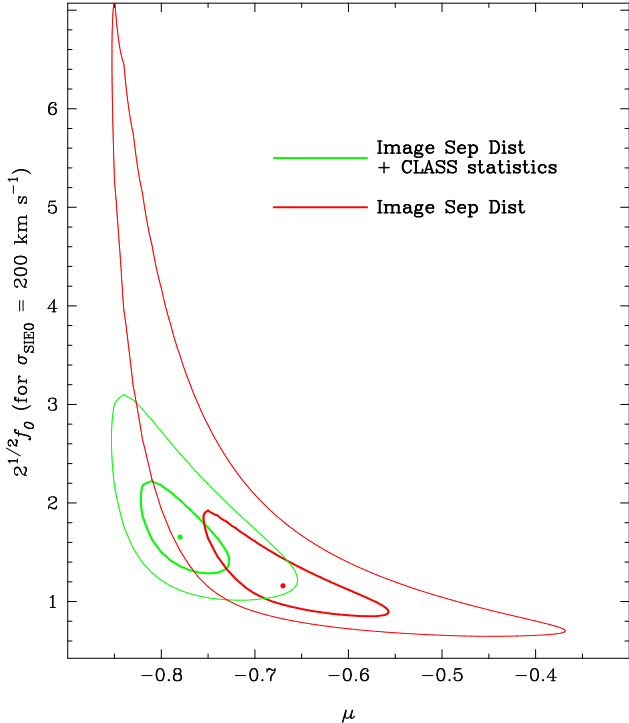


Figure 3. Likelihood contours in the plane of μ and $\sqrt{2}f_0$ based on strong lensing and semi-analytical model of galaxy formation. Here parameter μ is the power-law index in the model $f(v_{c,\text{vir}})$ (equation 6) for the ratio of the velocity dispersion (in the optical region and the inner halo) to the virial circular velocity and parameter f_0 is the value of the ratio at the fiducial velocity dispersion of $\sigma_{\text{SIE}0} = 200 \text{ km s}^{-1}$. The red contours are based only on the image separation distribution of radio lenses. The green contours are based on both the image separation distribution of radio lenses and all the lensing properties (including the lensing rate) of the CLASS statistical sample. The two contours for each case correspond respectively to the 68% and 95% confidence limits.

abundances of the early-type galaxies from the SAM have no effects on the constraints on the velocity profiles of galaxies. For this case we use all the lens systems used by Chae (2005), namely the 8 lens systems above along with the following 7 lens systems in the CLASS statistical sample; B0445+123, B0631+519, B0712+472, B1152+199, B1422+231, B1933+503, and B2319+051. The results for this case are also displayed in Figures 3 to 6.

Bearing in mind that the strict range of validity for our analyses is $200 \text{ km s}^{-1} \lesssim v_{c,\text{vir}} \lesssim 600 \text{ km s}^{-1}$ (see above), our main findings are as follows. First, parameter μ must be negative meaning that the ratio of the inner velocity to the virial velocity must be larger for a less massive halo (Fig. 3). A constant ratio (i.e. $\mu = 0$) is excluded at a highly significant level. We have $\mu = -0.78^{+0.05}_{-0.04}$ (68% CL) based on both the image separation distribution of radio lenses and the statistics of the CLASS statistical sample or $\mu = -0.67^{+0.11}_{-0.08}$ (68% CL) based only on the image separation distribution of radio lenses. Second, the inner velocity dispersion σ_{SIE} and the virial circular velocity $v_{c,\text{vir}}$ scale as

$$\frac{\sigma_{\text{SIE}}}{200 \text{ km s}^{-1}} = \frac{\eta \sigma_{\text{cent}}}{200 \text{ km s}^{-1}} = \left(1.17^{+0.40}_{-0.26} \frac{v_{c,\text{vir}}}{200 \text{ km s}^{-1}} \right)^{0.22^{+0.05}_{-0.04}} \quad (17)$$

for the case of using both the image separation distribution and CLASS statistics, or

$$\frac{\sigma_{\text{SIE}}}{200 \text{ km s}^{-1}} = \frac{\eta \sigma_{\text{cent}}}{200 \text{ km s}^{-1}} = \left(0.82^{+0.54}_{-0.18} \frac{v_{c,\text{vir}}}{200 \text{ km s}^{-1}} \right)^{0.33^{+0.11}_{-0.08}} \quad (18)$$

for the case of using only the image separation distribution. We take

$$\eta = \frac{\sigma_{\text{SIE}}}{\sigma_{\text{cent}}} = 1.0 \pm 0.1 \quad (19)$$

from Chae (2005) and Treu & Koopmans (2004). Third, for galaxies with velocity dispersion $\sigma_{\text{SIE}} \lesssim 210\text{-}230 \text{ km s}^{-1}$ the ratio $\sqrt{2}\sigma_{\text{SIE}}/v_{c,\text{vir}} (= v_{c,\text{eff}}/v_{c,\text{vir}})$ becomes increasingly larger than 1 as σ_{SIE} decreases (Fig. 4). For a typical bright galaxy with $\sigma_{\text{SIE}0} = 200 \text{ km s}^{-1}$, $\sqrt{2}f_0 = \sqrt{2}\sigma_{\text{SIE}0}/v_{c,\text{vir}0} = 1.65^{+0.57}_{-0.37}$ (image separation distribution + CLASS statistics) or $1.16^{+0.76}_{-0.30}$ (image separation distribution only) at the 68% confidence level. However, for large galaxies with $\sigma_{\text{SIE}} \gtrsim 210\text{-}230 \text{ km s}^{-1}$, the ratio $\sqrt{2}\sigma_{\text{SIE}}/v_{c,\text{vir}} \lesssim 1$. For a galaxy with $\sigma_{\text{SIE}} = 260 \text{ km s}^{-1}$, which corresponds approximately to $v_{c,\text{vir}} \sim 550 \text{ km s}^{-1}$ (see Fig. 5 and Fig. 6), $\sqrt{2}f = \sqrt{2}\sigma_{\text{SIE}}/v_{c,\text{vir}} = 0.65^{+0.15}_{-0.12}$ (image separation distribution + CLASS statistics) or $0.68^{+0.21}_{-0.11}$ (image separation distribution only) at the 68% confidence level. We discuss appropriate interpretations of these results along with possible sources of systematic errors in §4.

4 DISCUSSION

In this work we have compared the velocity dispersion at about the effective radius of the optical region (σ_{SIE}) derived from strong lensing based on the SIE lens model (equation 12) with the circular velocity at the virial radius of the surrounding halo ($v_{c,\text{vir}}$) predicted by semi-analytical studies of galaxy formation for the early-type galaxy population. Assuming that the inner velocity dispersion is related to the virial circular velocity by the simple power-law model (equation 6), we find that the ratio of the velocity dispersion to the circular velocity becomes increasingly larger as the velocity dispersion decreases; the power-law index μ in equation (6) must be negative (Fig. 3). Hence, we can conclude that there is clearly the trend that the smaller the surrounding halo is, the more enhanced the optical velocity dispersion is. This is the most robust result from our work. In addition to this, lensing studies (Kochanek 1994; Treu & Koopmans 2004; Chae 2005) have found that the velocity dispersion in the optical region derived from strong lensing based on singular isothermal ellipsoids, as is the case in this work, is about the same as the central stellar velocity dispersion determined from spectroscopic observations, namely $\eta = \sigma_{\text{SIE}}/\sigma_{\text{cent}} \approx 1$ (equation 19).

Strong lensing gives the scaling between the central velocity dispersion σ_{cent} and the virial circular velocity $v_{c,\text{vir}}$ as $\sigma_{\text{cent}} \propto v_{c,\text{vir}}^{0.22^{+0.05}_{-0.04}}$ (image separation distribution + CLASS statistics) or $\sigma_{\text{cent}} \propto v_{c,\text{vir}}^{0.33^{+0.11}_{-0.08}}$ (image separation distribution only). Our results are broadly consistent with those from recent other studies based on halo occupation statistics (Vale & Ostriker 2004; Yang et al. 2005) and galaxy-galaxy weak lensing (Mandelbaum et al. 2006).

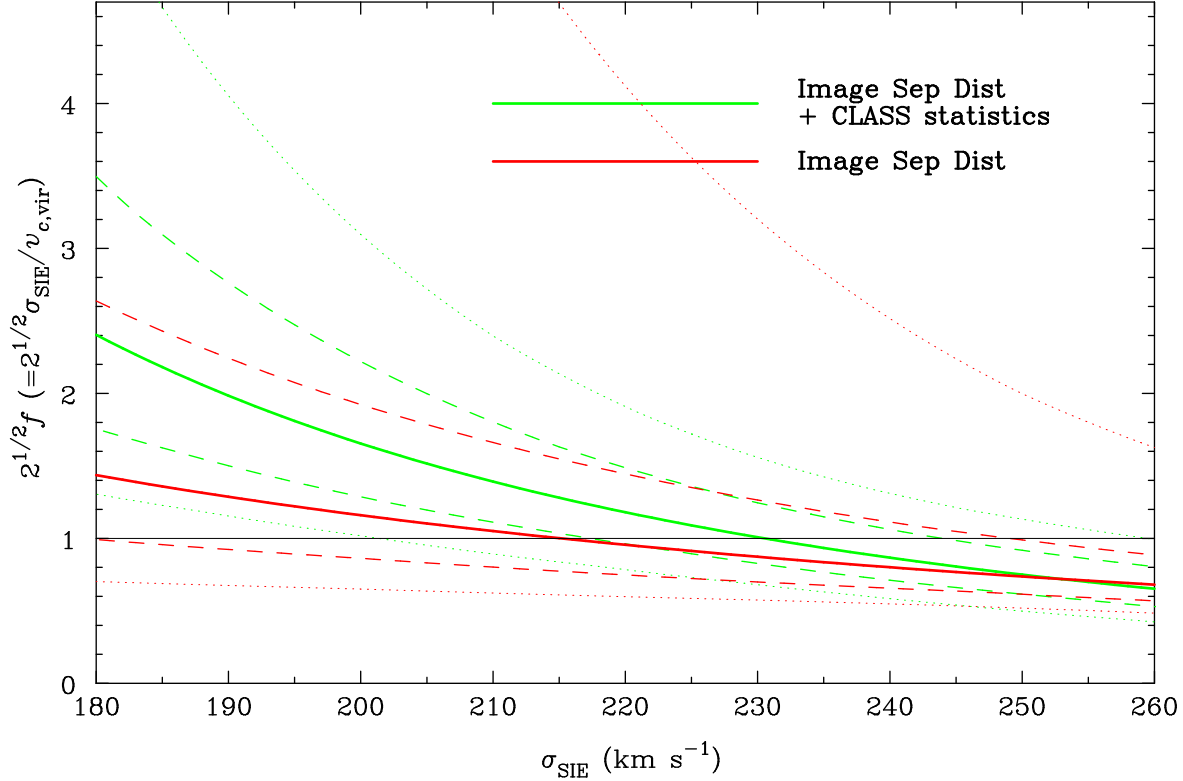


Figure 4. The behaviour of $\sqrt{2}f (= \sqrt{2}\sigma_{\text{SIE}}/v_{c,\text{vir}})$ as a function of σ_{SIE} . Here parameter σ_{SIE} is the velocity dispersion (in the optical region and the inner halo) implied by strong lensing assuming the singular isothermal ellipsoid model of Chae (2003) and parameter $v_{c,\text{vir}}$ is the circular velocity at the virial radius of the halo predicted by the Kang et al. (2005) semi-analytical model of galaxy formation. For our adopted model of the singular isothermal ellipsoid, the factor $\sqrt{2}\sigma_{\text{SIE}}$ corresponds to the circular velocity in the optical region and the inner halo $v_{c,\text{eff}}$. The red line is based only on the image separation distribution of radio lenses. The green line is based on both the image separation distribution of radio lenses and all the lensing properties (including the lensing rate) of the CLASS statistical sample. The dashed and dotted lines represent respectively the 68% and 95% confidence limits. Notice that the uncertainty in the ratio becomes larger at smaller velocity for a given uncertainty of the velocity.

These studies all obtained some relations between the virial mass of a halo M_{vir} and the luminosity L_c of a central galaxy hosted by the halo. Suppose $L_c \propto M_{\text{vir}}^{1/\gamma}$ and the Faber-Jackson relation (Faber & Jackson 1976) $L_c \propto \sigma^\beta$ where we shall take $\beta = 4$. It follows then $\sigma_{\text{cent}} \propto v_{c,\text{vir}}^{3/(\beta\gamma)}$ as $M_{\text{vir}} \propto v_{c,\text{vir}}^3$ (see Bullock et al. 2001). Vale & Ostriker (2004) found $\gamma \approx 3.57$ using halo occupation statistics for massive halos which implies $\sigma_{\text{cent}} \propto v_{c,\text{vir}}^{0.21}$. Using galaxy groups in the Two Degree Field Galaxy Redshift Survey, Yang et al. (2005) found $\gamma \approx 4$ for $M_{\text{vir}} \gtrsim 10^{13} h^{-1} M_\odot$ but $\gamma \approx 3/2$ for $M_{\text{vir}} \lesssim 10^{13} h^{-1} M_\odot$. The range of the halo mass corresponding to our velocity range extends across the transition mass $10^{13} h^{-1} M_\odot$, so the implied scaling will be somewhere between $\sigma_{\text{cent}} \propto v_{c,\text{vir}}^{0.19}$ and $\sigma_{\text{cent}} \propto v_{c,\text{vir}}^{0.5}$. The galaxy-galaxy weak lensing study of Mandelbaum et al. (2006) found $\gamma \approx 2.7$ for galaxies with $L_c \gtrsim L_*$ which implies $\sigma_{\text{cent}} \propto v_{c,\text{vir}}^{0.28}$. All these results are clearly consistent with our results within the statistical errors.

Our plot (Fig. 4) of the ratio $\sqrt{2}f (= \sqrt{2}\sigma_{\text{SIE}}/v_{c,\text{vir}} = v_{c,\text{eff}}/v_{c,\text{vir}})$ (equation 5; where σ_{SIE} is the velocity dispersion at about the effective radius and $v_{c,\text{vir}}$ is the circular velocity at the virial radius) against the velocity dispersion σ_{SIE} shows some interesting features. First of all, for

galaxies with velocity dispersion $\sigma_{\text{SIE}} \lesssim 210\text{-}230 \text{ km s}^{-1}$ the ratio $\sqrt{2}f > 1$. For example, a typical bright galaxy with $\sigma_{\text{SIE0}} = 200 \text{ km s}^{-1}$ has $\sqrt{2}f_0 = 1.65^{+0.57}_{-0.37}$ (image separation distribution + CLASS statistics) or $1.16^{+0.76}_{-0.30}$ (image separation distribution only). Given $v_{c,\text{eff}} = \sqrt{2}\sigma$ for our lens model (equation 12), the above results are in agreement with the Seljak (2002) galaxy-galaxy weak lensing result of $v_{c,\text{opt}}/v_{c,\text{vir}} = 1.68 \pm 0.2$ for an L_* early-type galaxy with his adopted value of $\sigma_{\text{cent}} = 177 \text{ km s}^{-1}$.³ A striking feature of Fig. 4 is its behaviour at high velocity dispersions. The ratio $\sqrt{2}f$ is about 1 or less for $\sigma_{\text{SIE}} \gtrsim 210\text{-}230 \text{ km s}^{-1}$. For a galaxy with $\sigma_{\text{SIE}} = 260 \text{ km s}^{-1}$, which is hosted by a halo of $v_{c,\text{vir}} \sim 550 \text{ km s}^{-1}$ (see Fig. 6), our result is $\sqrt{2}f = 0.65^{+0.15}_{-0.12}$ (image separation distribution + CLASS statistics) or $0.68^{+0.21}_{-0.11}$ (image separation distribution only) at 68% confidence level. The 95% confidence range is $0.42 \leq \sqrt{2}f \leq 0.99$ (image separation distribution + CLASS statistics) or $0.48 \leq \sqrt{2}f \leq 1.63$ (image separation

³ It appears that the value of $v_{c,\text{opt}}/v_{c,\text{vir}}$ changes little between $\sigma_{\text{cent}} = 177 \text{ km s}^{-1}$ and 200 km s^{-1} according to the results by Seljak (2002).

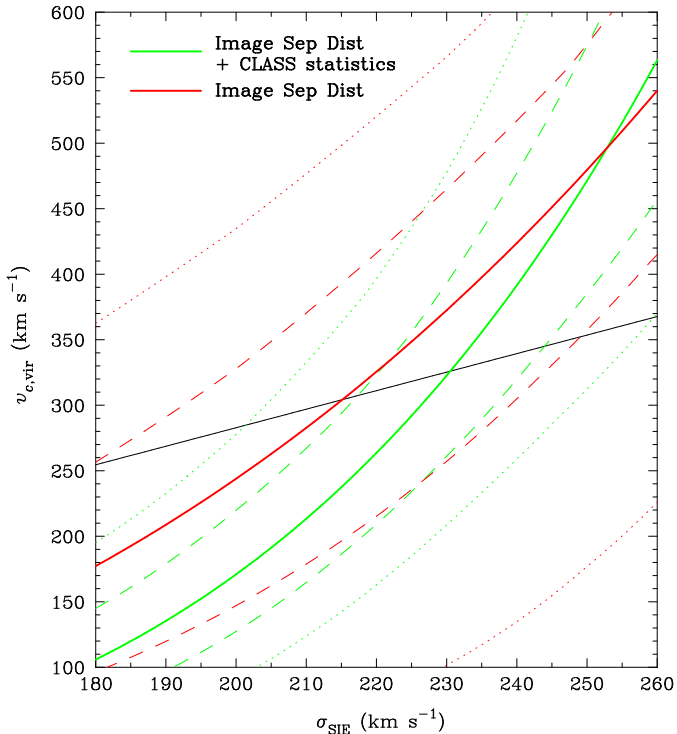


Figure 5. The behaviour of $v_{c,\text{vir}}$ as a function of σ_{SIE} . Here parameters $v_{c,\text{vir}}$ and σ_{SIE} are the same as in Fig. 4. The red and green lines are also the same as in Fig. 4. The dashed and dotted lines represent respectively the 68% and 95% confidence limits. The solid black line represents $v_{c,\text{vir}} = \sqrt{2}\sigma_{\text{SIE}}$. Notice that the uncertainty in $v_{c,\text{vir}}$ is nearly unchanged as σ_{SIE} is varied.

distribution only) for $\sigma_{\text{SIE}} = 260 \text{ km s}^{-1}$. From Seljak (2002) $\sqrt{2}f = 1.3 \pm 0.2$ for $\sigma_{\text{cent}} = 290 \text{ km s}^{-1}$. Given that our derived velocity dispersion σ_{SIE} is believed to be similar to the central stellar velocity dispersion σ_{cent} (equation 19), our results and the Seljak (2002) results show some intriguing difference although the 95% statistical errors partially overlap. For the large circular velocity systems ($v_{c,\text{vir}} \sim 550 \text{ km s}^{-1}$), it is likely that the haloes may host several galaxies and our inner velocity dispersion is appropriate for a central galaxy. One possible interpretation of our results is then that the optical galaxy is well within the peak radius r_{peak} where the circular velocity is highest and the baryonic boost of the velocity within the optical galaxy is relatively small for the halo with $v_{c,\text{vir}} \sim 550 \text{ km s}^{-1}$ (see below for further discussion).

While our results appear to be in reasonable agreement with halo occupation number studies of Vale & Ostriker (2004) and Yang et al. (2005) and the most recent weak lensing studies of Mandelbaum et al. (2006), it is still important to consider possible sources of systematic errors for our results. First of all, the abundances of early-type galaxies at low virial circular velocities from the SAM are uncertain at present. As can be seen in Fig. 1, the abundances of early-type galaxies from the SAM appear to be abnormally high at low virial circular velocities and do not fit into our model CVF. In fact, Kang et al. (2005) find that their predicted luminosity function of early-type galaxies does not match well

observed luminosity functions at the low end of luminosity. Semi-analytical methods have their limitations primarily due to uncertainties in the star formation and feedback processes (which are also present in hydrodynamical simulations). In most semi-analytical studies it appears that the number of galaxies at the faint end tends to increase faster than the observed trend as the luminosity decreases. We have chosen to ignore the lowest four data points of the SAM (Table 2) in fitting our model CVF. As far as our analyses are limited to the range $200 \text{ km s}^{-1} \lesssim v_{c,\text{vir}} \lesssim 600 \text{ km s}^{-1}$, ignoring the lowest four data points would not affect the results based on the image separation distribution only. However, ignoring the lowest four data points may cause a systematic error for the results based on both the image separation distribution and CLASS statistics because the lensing rate depends on the entire range of the velocity dispersion function but discounting the four data points may have biased the behaviour of the circular velocity function so that the relation between the two may be affected. Nevertheless, it is likely that the systematic error might not be too large for the following reasons. Our procedure does not entirely ignore the low circular velocity galaxies but uses the extrapolated abundances from the fitted function rather than the given abundances. Moreover, current observations show that as the luminosity of the early-type galaxy decreases below L_* the surface brightness distribution becomes less concentrated so that it is less effective for strong lensing.

Secondly, the abundances of early-type galaxies at the highest velocity end might also be systematically biased. In fact, semi-analytical models tend to over-predict the number of very luminous galaxies, although the inclusion of AGN feedbacks seems to cure this problem (Bower et al. 2006; Croton et al. 2006). An over-predicted abundance of galaxies at a given virial circular velocity will lead to an underestimate of f at the corresponding velocity dispersion. To see this effect we have done the following numerical experiment. We decreased the numbers of early-type galaxies for bins $i = 9$ to 15 in Table 1 (with $v_{c,\text{vir}} > 312.5 \text{ km s}^{-1}$) by successively larger proportions from $i = 9$ to 15 so that at $i = 15$ the adjusted number becomes one half of the unadjusted number. In this case we indeed find that the value of f somewhat increases at large velocity dispersions in particular at $\sigma_{\text{SIE}} = 260 \text{ km s}^{-1}$ but within the 68% statistical error.

Thirdly and finally, our results might be biased because of the assumed lens model, namely the SIE (equation 12). Theoretically, the circular velocity (or the velocity dispersion) derived from strong lensing depends on the radial profile and the shape of the model mass distribution. For the observed image size and morphology, the predicted size of the Einstein ring R_{Ein} and the projected mass within the ring M_{Ein} depend on the radial profile. However, for most of the known lens systems detailed mass modelling shows that the derived R_{Ein} and M_{Ein} vary little as the radial profile is varied. The circular velocity at R_{Ein} depends on the mass within the sphere of radius R_{Ein} , $M(R_{\text{Ein}})$ rather than M_{Ein} . For a spherical mass distribution of the form $\rho \sim r^{-\nu}$ a model with $\nu = 1.7$ ($\nu = 2.3$) would give a circular velocity at $r = R_{\text{Ein}}$ 12% lower (9% higher) than the isothermal model with $\nu = 2$ for the same M_{Ein} . It is possible that the average mass profile of early-type galaxies systematically varies from smaller systems to larger systems. In fact, our own results appear to

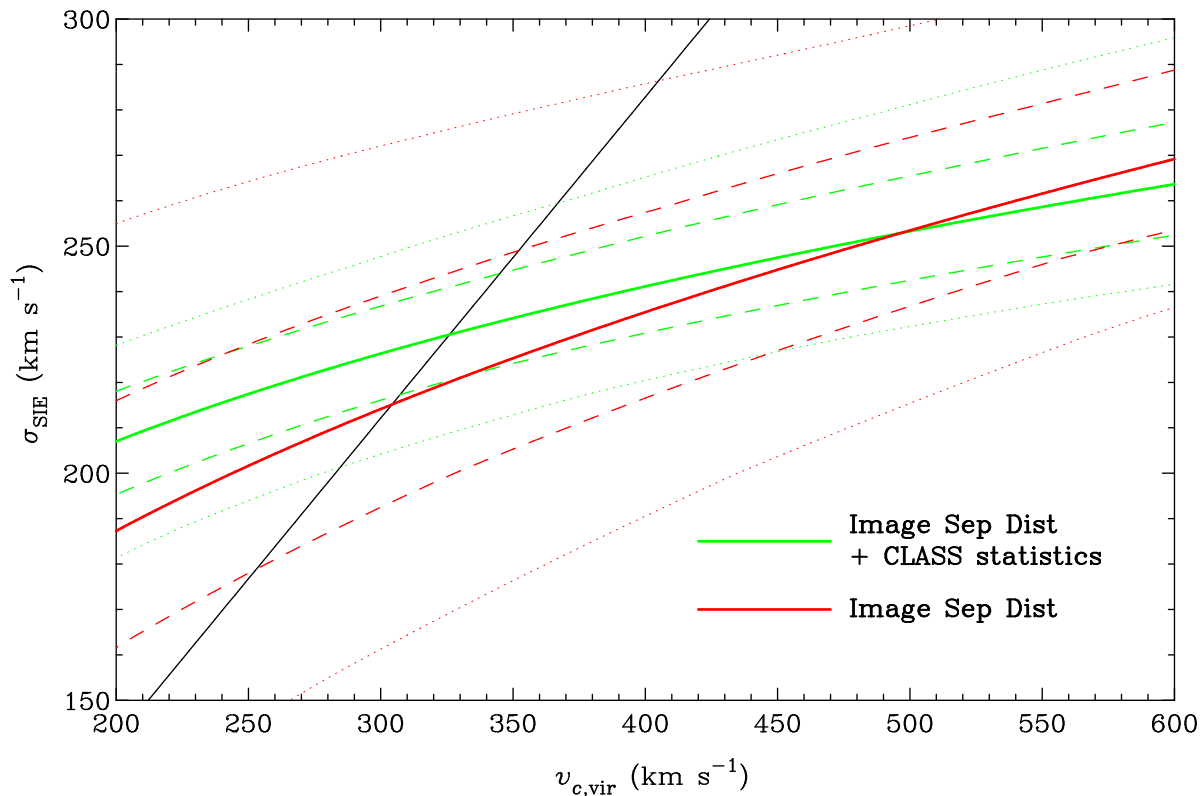


Figure 6. The behaviour of σ_{SIE} as a function of $v_{\text{c,vir}}$. Notations are the same as in Fig. 5.

imply varying structures of early-type galaxies (see below). Nevertheless, the errors for f arising from approximating all the galaxies using isothermal models appear to be within the current 68% statistical errors. Furthermore, the inner mass profiles of early-type galaxies at least up to the effective radii appear to be close to isothermal from stellar dynamical modelling (e.g., Rix et al. 1997; Thomas et al. 2005) as well as from detailed modelling of individual lenses (e.g., Rusin & Kochanek 2005; Koopmans et al. 2006). Thus, the assumption of the SIE model might not actually cause as large errors as estimated above. The shape of the mass distribution also affects the derived circular velocity (or velocity dispersion) from strong lensing. For example, prolate and oblate isothermal models give different results (see Chae 2003). In this work we have assumed that one half of galaxies are oblate and the other half are prolate. The average shape of early-type galaxies might systematically vary from smaller systems to larger systems. However, according to the model of Chae (2003) the change of the velocity dispersion from the half oblate and half prolate case is $\sim 10\%$ even for the extreme cases of all oblate and all prolate. Considering the above estimates of possible systematic errors, we can tentatively conclude that the essential trend of f for $200 \text{ km s}^{-1} \lesssim v_{\text{c,vir}} \lesssim 600 \text{ km s}^{-1}$ and the result $\sqrt{2}f \lesssim 1$ at $\sigma_{\text{SIE}} = 260 \text{ km s}^{-1}$ are likely to be real.

The fact that $\sqrt{2}f (= v_{\text{c,eff}}/v_{\text{c,vir}})$ is not unity shows that galaxies are not well approximated by isothermal profiles for significant parts of the virial radii. The trend of f as a function of the velocity dispersion constrained from strong

lensing in this work is in agreement with theoretical expectations. First, more massive haloes have smaller concentrations (see Navarro et al. 1997; Bullock et al. 2001), and so they have smaller peak velocities relative to the virial circular velocity compared with smaller haloes. Second, the baryonic modifications to the inner mass profiles of the haloes are less pronounced for more massive haloes and consequently the baryonic boost of the velocity may be smaller. On the other hand, smaller circular velocity systems may have a larger value of f as baryonic cooling could be more efficient in such systems (although feedback processes may suppress cooling in very small systems). Third, for massive haloes the radius of the optical galaxy may be much smaller than the peak radius r_{peak} of the halo where the circular velocity obtains its maximum while the optical radius is comparable to r_{peak} for small haloes. However, to assess the full significance of our results, detailed modelling is necessary incorporating theoretical halo profiles, baryonic modifications of the haloes, observed light distributions and realistic distribution functions (see, e.g., van der Marel et al. 2000 for modelling of galaxy clusters).

In this work, we consider only a simple two-component model recently used in the literature (Keeton 2001; Seljak 2002) to see whether our derived ratio of the SIE velocity dispersion to the virial circular velocity can be matched qualitatively and shed new light on galactic structures. (We postpone a more detailed work to a future publication.) The model starts from an initial NFW halo and then turns into a Hernquist (Hernquist 1990) light (stellar mass) dis-

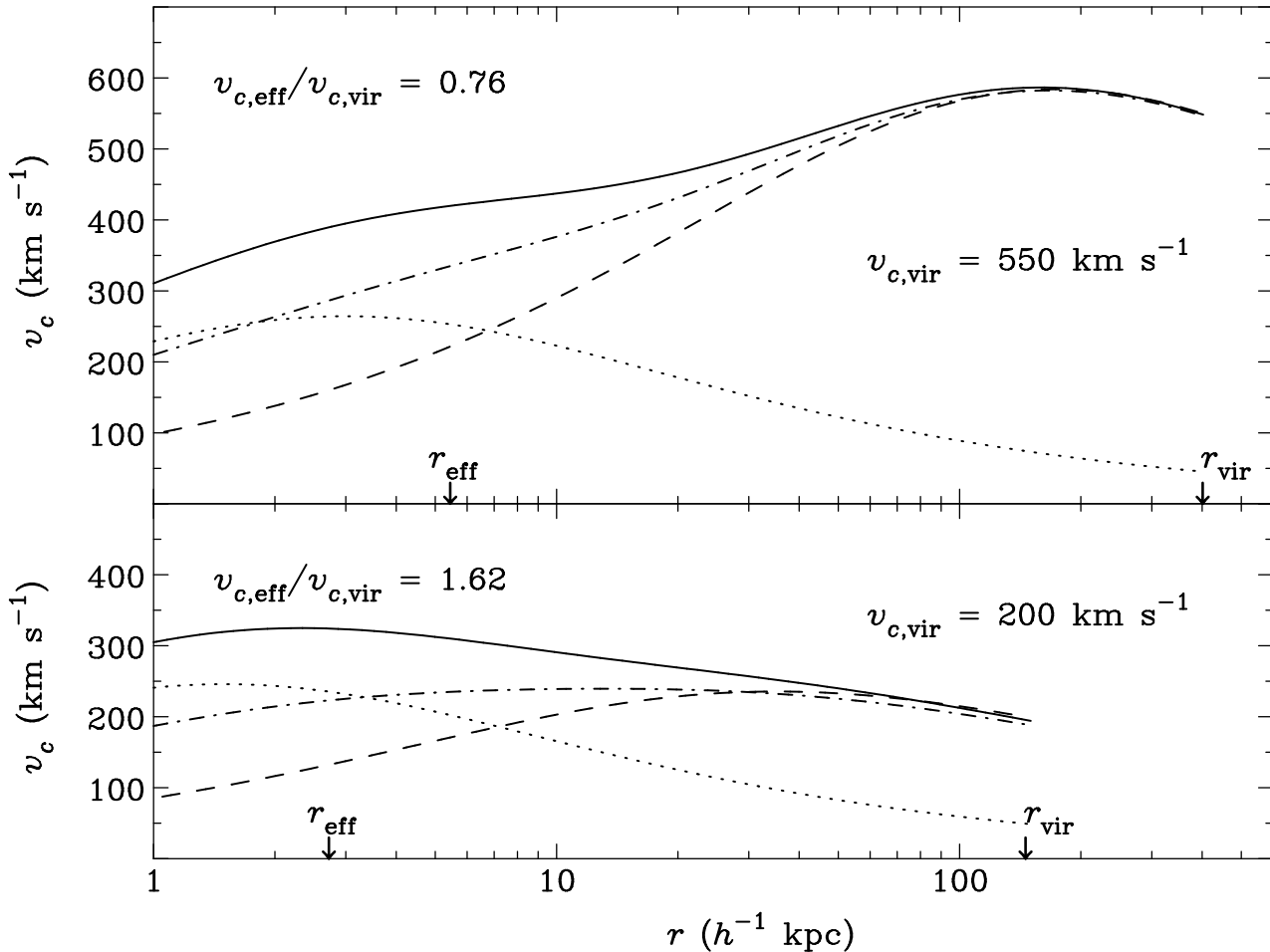


Figure 7. The circular velocity profiles for a two-component early-type galaxy model at $z = 0.6$ consisting of a Hernquist light (stellar mass) distribution residing in a halo, which is supposed to form from an initial NFW halo by baryonic cooling. The solid, dashed, dash-dotted, and dotted lines represent respectively the profiles for the final total mass, initial NFW halo, final modified halo, and Hernquist stellar mass distributions. For the lower panel ($v_{c,\text{vir}} = 200 \text{ km s}^{-1}$), we take $c_{\text{vir}} = 9$ and $F_{\text{cool}} = 0.09$. For the upper panel ($v_{c,\text{vir}} = 550 \text{ km s}^{-1}$), we take $c_{\text{vir}} = 5$ and $F_{\text{cool}} = 0.01$. Here c_{vir} is the halo concentration (Bullock et al. 2001) and F_{cool} is the fraction of cooled baryons forming stars out of the initial total mass. In these models, the predicted ratios of the circular velocities at the effective and the virial radii $v_{c,\text{eff}}/v_{c,\text{vir}}$ are consistent with our derived values of $\sqrt{2}\sigma_{\text{SIE}}/v_{c,\text{vir}}$.

tribution by baryonic infall residing in a modified halo. We use the adiabatic contraction model by Blumenthal et al. (1986) to calculate the modified halo profile. Fig. 7 shows the constructed models at redshift $z = 0.6$ for the haloes of $v_{c,\text{vir}} = 200 \text{ km s}^{-1}$ and $v_{c,\text{vir}} = 550 \text{ km s}^{-1}$. For the $v_{c,\text{vir}} = 200 \text{ km s}^{-1}$ halo, we take $c_{\text{vir}} = 9$ (where c_{vir} is the halo concentration) and $F_{\text{cool}} = 0.09$ (where F_{cool} is the the cooled baryon fraction out of the total mass). For the $v_{c,\text{vir}} = 550 \text{ km s}^{-1}$ halo, $c_{\text{vir}} = 5$ and $F_{\text{cool}} = 0.01$. Here we have (approximately) estimated the values of c_{vir} using the simulation results of Bullock et al. (2001) while the values of F_{cool} have been adjusted to produce circular velocity functions that are consistent with the results from this work. Consequently, in these models the predicted values of the ratio of the circular velocities at the effective and the virial radii $v_{c,\text{eff}}/v_{c,\text{vir}}$ are in agreement with our derived

values of $\sqrt{2}f$ for $\sigma_{\text{SIE}} = 200 \text{ km s}^{-1}$ and 260 km s^{-1} . The circular velocity curves shown in Fig. 7 imply evidently the following for galaxy formation processes and resultant mass profiles. First, the galaxies with $v_{c,\text{vir}} = 200 \text{ km s}^{-1}$ (and corresponding $\sigma_{\text{SIE}} = 200 \text{ km s}^{-1}$) and $v_{c,\text{vir}} = 550 \text{ km s}^{-1}$ ($\sigma_{\text{SIE}} = 260 \text{ km s}^{-1}$) require very different values of F_{cool} in order to be consistent with our derived values of $\sqrt{2}f$. The fitted values of F_{cool} imply that the fraction of infalling baryons forming stars and consequential modification to the halo are becoming increasingly smaller as the halo gets more and more massive. This is qualitatively consistent with the fact that for galaxy clusters (the high mass limit of haloes) the NFW halo profile is well preserved. Second, the system of $v_{c,\text{vir}} = 200 \text{ km s}^{-1}$ has a density profile close to isothermal up to a few effective radii but steeper than isothermal beyond. On the other hand, the system of $v_{c,\text{vir}} = 550 \text{ km s}^{-1}$

has a profile shallower than isothermal up to about a half of the virial radius. However, more detailed investigations along with more precise interpretations will be considered in a future publication.

The parameterisation we use in equation (6) might not be optimal. The current CLASS and PANELS samples are, however, too small to allow us to explore a more realistic functional form. However, one advantage of the method is worth emphasizing: the lensing probability scales as f^4 and the separation scales as f^2 – the lensing properties therefore depends on quite high powers of f . This also implies that even if the semi-analytical modelling is somewhat uncertain, we may still be able to put strong limits on this parameter with the next-generation lens surveys. Current generation hydrodynamical simulations cannot yet resolve and simulate the inner parts of early-type galaxies realistically. For example, the high resolution simulation of an early-type galaxy by Meza et al. (2003) predicts a central velocity dispersion as high as 650 km s^{-1} due to the compact size of their stellar component. So gravitational lensing can play an important role in empirically assessing the roles of baryonic cooling in galaxy formation and evolution.

We thank Yipeng Jing and Ian Browne for helpful discussions. We also thank the anonymous referee for insightful comments that greatly improved the presentation and discussion. KHC acknowledges support from the Astrophysical Research Center for the Structure and Evolution of the Cosmos by KOSEF. SM was partly supported in travel by the Chinese Academy of Sciences and the European Community's Sixth Framework Marie Curie Research Training Network Programme, Contract No. MRTN-CT-2004-505183 "ANGLES". KX acknowledges a fellowship from the Royal Society and travel support from Jodrell Bank.

REFERENCES

- Blumenthal G. R., Faber S. M., Flores R., Primack J. R., 1986, *ApJ*, 301, 27
- Bond J. R., Cole S., Efstathiou G., Kaiser N., 1991, *ApJ*, 379, 440
- Bower R. G., Benson A. J., Malbon R., Helly J. C., Frenk C. S., Baugh C. M., Cole S., Lacey C. G., 2006, *MNRAS*, 370, 645
- Bullock J. S., Kolatt T. S., Sigad Y., Somerville R. S., Kravtsov A. V., Klypin A. A., Primack J. R., Dekel A., 2001, *MNRAS*, 321, 559
- Browne I. W. A. et al., 2003, *MNRAS*, 341, 13
- Chae K.-H., 2003, *MNRAS*, 346, 746
- Chae K.-H., 2005, *ApJ*, 630, 764
- Chae K.-H. et al., 2002, *Phys. Rev. Lett.*, 89, 151301
- Chae K.-H., Mao S., 2003, *ApJ*, 599, L61
- Cole S., Lacey C. G., Baugh C. M., Frenk C. S., 2000, *MNRAS*, 319, 168
- Comerford J. M., Meneghetti M., Bartelmann M., Schirmer M., 2006, *ApJ*, 642, 39
- Croton D. J., Springel V., White S. D. M., de Lucia G., Frenk C. S., Gao L., Jenkins A., Kauffmann G., Navarro J. F., Yoshida N., 2006, *MNRAS*, 365, 11
- de Blok W. J. G., 2005, *ApJ*, 634, 227
- Faber S. M., Jackson R. E., 1976, *ApJ*, 204, 668
- Fassnacht C. D. et al., 1999, *AJ*, 117, 658
- Fukugita M., Futamase T., Kasai M., Turner E. L., 1992, *ApJ*, 393, 3
- Helbig P., Marlow D., Quast R., Wilkinson P. N., Browne I. W. A., Koopmans L. V. E., 1999, *A&AS*, 136, 297
- Hernquist L., 1990, *ApJ*, 356, 359
- Jing Y. P., Suto Y., 2002, *ApJ*, 574, 538
- Kang X., Jing Y. P., Mo H. J., Börner G., 2005, *ApJ*, 631, 21
- Kauffmann G., Colberg J. M., Diaferio A., White S. D. M., 1999, *MNRAS*, 307, 529
- Keeton C. R., 2001, *ApJ*, 561, 46
- Kochanek C. S., 1994, *ApJ*, 436, 56
- Kochanek C. S., 1995, *ApJ*, 453, 545
- Kochanek C. S., 1996, *ApJ*, 466, 638
- Koopmans L. V. E., Treu T., Bolton A. S., Burles S., Moustakas L. A., 2006, *ApJ*, 649, 599
- Lacey C., Cole S., 1994, *MNRAS*, 271, 676
- Mandelbaum R., Seljak U., Kauffmann G., Hirata C. M., Brinkmann J., 2006, *MNRAS*, 368, 715
- Mao S., 1991, *ApJ*, 380, 9
- Mao S., Kochanek C. S., 1994, *MNRAS*, 268, 569
- Marzke R. O., da Costa L. N., Pellegrini P. S., Willmer C. N. A., Geller M. J., 1998, *ApJ*, 503, 617
- Meza A., Navarro J. F., Steinmetz M., Eke V. R., 2003, *ApJ*, 590, 619
- Mitchell J. L., Keeton C. R., Frieman J. A., Sheth R. K., 2005, *ApJ*, 622, 81
- Myers S. T. et al., 2003, *MNRAS*, 341, 1
- Narayan R., White S. D. M., 1988, *MNRAS*, 231, 97
- Navarro J. F., Frenk C. S., White S. D. M., 1997, *ApJ*, 490, 493
- Navarro J. F., Hayashi E., Power C., Jenkins A. R., Frenk C. S., White S. D. M., Springel V., Stadel J., Quinn T. R., 2004, *MNRAS*, 349, 1039
- Ofek E. O., Rix H.-W., Maoz D., 2003, *MNRAS*, 343, 639
- Peacock J. A. et al., 2001, *Nature*, 410, 169
- Press W. H., Schechter P., 1974, *ApJ*, 187, 425
- Rix H.-W., de Zeeuw P. T., Cretton N., van der Marel R. P., Carollo C. M., 1997, *ApJ*, 488, 702
- Rusin D., Kochanek C. S., 2005, *ApJ*, 623, 666
- Schechter P., 1976, *ApJ*, 203, 297
- Seljak U., 2002, *MNRAS*, 334, 797
- Sheth R. K., Tormen G., 2002, *MNRAS*, 329, 61
- Sheth R. K. et al., 2003, *ApJ*, 594, 225
- Simien F., de Vaucouleurs G., 1986, *ApJ*, 302, 564
- Somerville R. S., Primack J. R., 1999, *MNRAS*, 310, 1087
- Spergel D. N. et al., 2003, *ApJS*, 148, 175
- Spergel D. N. et al., 2006, preprint (astro-ph/0603449)
- Springel V., Hernquist L., 2003, *MNRAS*, 339, 289
- Swaters R. A., Madore B. F., van den Bosch F. C., Balcells M., 2003, *ApJ*, 583, 732
- Tegmark M. et al., 2004, *ApJ*, 606, 702
- Thomas J., Saglia R. P., Bender R., Thomas D., Gebhardt K., Magorrian J., Corsini E. M., Wegner G., 2005, *MNRAS*, 360, 1355
- Treu T., Koopmans L. V. E., 2004, *ApJ*, 611, 739
- Turner E. L., Ostriker J. P., Gott J. R., III, 1984, *ApJ*, 284, 1
- Vale A., Ostriker J. P., 2004, 353, 189

- van der Marel R. P., Magorrian J., Carlberg R. G., Yee H. K. C., Ellingson E., 2000, *AJ*, 119, 2038
- Voigt L. M., Fabian A. C., 2006, *MNRAS*, 368, 518
- Winn J. N. et al., 2000, *AJ*, 120, 2868
- Winn J. N., Lovell J. E. J., Chen H.-W., Fletcher A. B., Hewitt J. N., Patnaik A. R., Schechter P. L., 2002a, *ApJ*, 564, 143
- Winn J. N., Morgan N. D., Hewitt J. N., Kochanek C. S., Lovell J. E. J., Patnaik A. R., Pindor B., Schechter P. L., Schommer R. A., 2002b, *AJ*, 123, 10
- Winn J. N., Hewitt J. N., Patnaik A. R., Schechter P. L., Schommer R. A., López S., Maza J., Wachter S., 2001a, *AJ*, 121, 1223
- Winn J. N., Hewitt J. N., Schechter P. L., 2001b, in *Gravitational Lensing: Recent Progress and Future Goals*, ASP Conference Proceedings, Vol. 237, ed. T. G. Brainerd & C. S. Kochanek (San Francisco: ASP), p. 61
- Yang X., Mo H. J., Jing Y. P., van den Bosch F. C., 2005, *MNRAS*, 358, 217